Small-Angle X-ray Scattering Experiments in Grazing Incidence on Sol–Gel Coatings Containing Nano-Scaled Gold Colloids: a New Technique for Investigating Thin Coatings and Films

B. KUTSCH,[a] O. LYON,[b] M. SCHMITT,[a] M. MENNIG[a] AND H. SCHMIDT[a]

[a] *Institut für Neue Materialien, Im Stadtwald, Gebäude 43, D-66123 Saarbrücken, Germany, and* [b] *Laboratoire pour l'Utilisation du Rayonnement Électromagnétique (LURE), Bâtiment 209D, Centre Universitaire Paris-Sud, F-91405 Orsay, France. E-mail: kutsch@inm-gmbh.de*

Abstract

Small-angle X-ray scattering (SAXS) is generally not applicable to thin (~ 1 μm) films and coatings because of their weak scattering signal in conventional transmission experiments. This restriction can be overcome by working in grazing incidence, with an angle of incidence α slightly above the critical angle of total reflection φ_c, in order to augment the effective X-ray path in the sample. The possibilities of this technique are demonstrated by preliminary results obtained on glass-like sol–gel coatings containing nano-scaled gold colloids. The scattering of the gold colloids was identified by variations of the X-ray energy near the absorption edge of gold (anomalous SAXS). It showed the theoretically predicted variation of intensity with energy. The recorded scattering spectra were corrected for absorption and refraction effects, whose influences on the spectra are discussed. Calculated size distributions of the colloids from SAXS in grazing incidence were compared with results from high-resolution transmission electron microscopy (HTEM) investigations and optical UV–visible spectroscopy.

1. Introduction

The analysis of the electronic structure of materials such as alloys, glasses, microemulsions and gels by small-angle X-ray scattering (SAXS) and anomalous SAXS (ASAXS) in order to obtain information about fluctuations of their electronic density is of great interest in materials research. Typical questions in this field concern phase-separation problems, colloidal precipitations or nano-scaled variations in electronic density, growth mechanisms of colloids and network formation in sol–gel systems. Recent reviews may be found in the work of Naudon (1995) and Materlik, Sparks & Fisher (1994).

This study concentrates on the experimental aspects of (A)SAXS in grazing incidence. The technique was applied to thermally densified glass-like sol–gel coatings containing nano-scaled gold colloids on glass substrates in order to demonstrate its possibilities in the investigation of thin films and coatings, and to obtain information on their electronic structure. The thickness of the coatings was between 1.1 and 2 μm. The embedded colloids were formed *in situ* during densification of the matrix by thermal reduction of complexed gold ions added to the sol (Spanhel, Mennig & Schmidt, 1992; Schmitt, 1997). These sol–gel materials offer a wide range of optical and decorative applications and were recently found to have promising nonlinear optical properties (Mennig, Becker, Jung & Schmidt, 1994) which are strongly affected by the stabilizer used in the sol. The gold system was selected because of the high scattering contrast between gold and the matrix, and because the size of the colloids lay within the detectable size range; it was used for feasibility studies and the first experiments in grazing incidence. SAXS experiments were performed in grazing incidence using an angle of incidence α of 0.3°, which leads to an augmentation of the effective X-ray path in the sample by a factor of about 200. This technique was developed some years ago by Naudon, Slimani & Goudeau (1991) who applied it in two feasibility studies to tungsten carbide layers and an Ag–Al alloy (Slimani, Goudeau, Naudon, Farges & Derep, 1991).

2. Experimental set-up

The experiments were performed at the beamline D22 at LURE, which is described in detail by Dubuisson, Dauvergne, Depautex, Vachette & Williams (1986) and Materlik, Sparks & Fischer (1994); only special features of the experimental set-up will be described here. The incident X-ray beam was collimated to a height of 100 μm and a width of 1 mm; it struck the sample holder for grazing incidence (Fig. 1) under an angle of incidence α of 0.3° in the centre of a cylindrical chamber, which was linked to the entrance slits and to the detector. The whole system was kept under a vacuum or below 10 Pa. The sample holder could be rotated in an arbitrary way to modify α and shift the height of y by

± 7 mm. Applying an α of 0.3°, which is about 0.08–0.11° above the critical angle of total reflection φ_c for the samples, avoids total refraction of the X-rays at the sample surface and confinement of the totally refracted wavefield inside the top 5–20 nm of the coating (Levine, Cohen & Chung, 1991). Thus X-rays can penetrate the coatings for investigation of their bulk properties. Because of the surface roughness of the coatings, which is in the order of several nanometers, experiments below φ_c would not be meaningful, but in principle are also possible with the present set-up.

The precision of α was about 0.01°; the accuracy for y was better than 5 μm. As fixed by the geometry of the sample holder, the sample surface is always mounted in the same position independent of its thickness. The accessible surface size of the sample for the incident beam was about 8×40 mm. A first beam-stop (distance 260 mm, height 1 mm) to cover the incident transmitted beam could be rotated in a concentric way around the sample. Directly in front of the detector, a second beam-stop was installed perpendicularly to the first one in order to cover the part of the incident beam that was reflected at the surface of the sample. All adjustments and movements of the beam-stops and the sample holder were remote-controlled. As detector, a two-dimensional position-sensitive proportional counter with an Xe–CH_4 mixture was used. It had 256 channels in each direction and a space resolution of 0.334×0.334 mm. The sample-to-detector distance was 657 mm. For precise angular adjustment of the set-up, an additional collimator was mounted on the sample holder without a sample. It left only a small slit of 100 μm in height parallel to the usual position of the sample surface in order to find exactly the zero position α_0 of α and to adjust the height of the sample holder y at $\alpha = 0$ by filling its slit with the incident beam. Finally, the sample holder was lifted by 50 μm to cut exactly half of the incident intensity.

To find the critical angle φ_c of the sample, α was varied around α_0, leading to a strongly increasing intensity as the angle φ_c was approached (see Fig. 2). Its onset was at 0.22 ± 0.03° for all samples described in this study. To avoid strong total reflection and to ensure that the incident beam enters the coating, the angle of incidence was then increased to 0.3°. This prevents small deviations of α leading to a drastic change in the transmitted intensity.

The scattering spectra recorded after these procedures and after mounting the two-dimensional detector showed nearly spherical symmetry around the origin of the detector which was determined separately. An example of such a spectrum is given in Fig. 3. The two perpendicular bars indicate the regions covered by the beam-stops. During regular checks of the geometry of the experiment, it was observed that height and angle of incidence of the incoming beam at D22 varied sometimes after a new injection by a few hundredths of a mm or of a degree, respectively. Thus, the adjustment of α_0, y_0 and $2\theta_0$ had to be checked regularly. Finally,

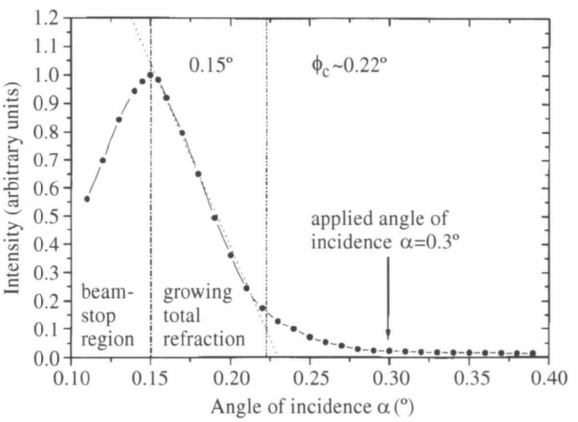

Fig. 2. Variation of the detected intensity as a function of the angle of incidence α after adjustment of α_0 and y_0.

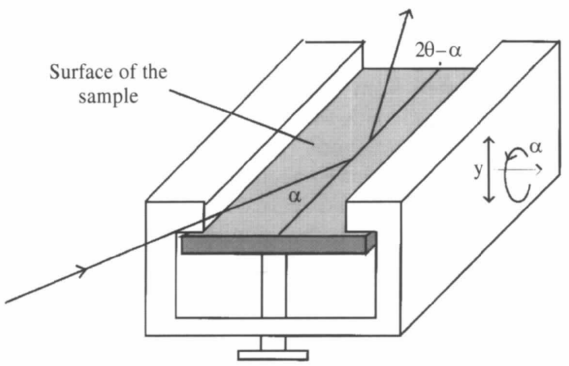

Fig. 1. Schematic representation of the rotatable sample holder used for experiments in grazing incidence.

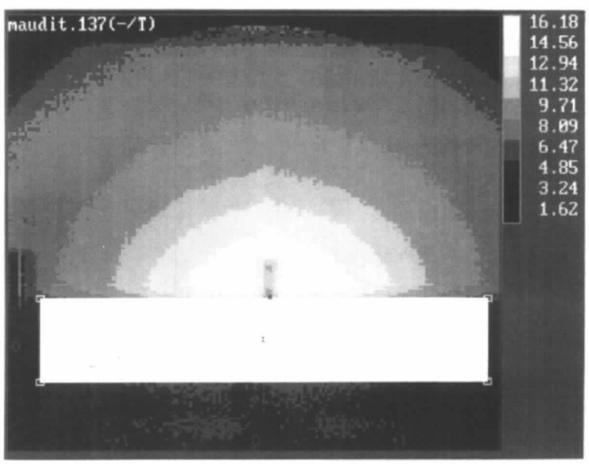

Fig. 3. Two-dimensional spectrum in grazing incidence (log intensity scale) after corrections ($\alpha = 0.3$°, $E = 8050$ eV) of a sol–gel coating with nano-scaled Au colloids (Au:DIAMO = 1:4) densified at 423 K.

because of the symmetry of the spectra after absorption and refraction corrections, they were integrated within concentric spheres around the origin to improve the statistics and to obtain one-dimensional curves for easier data analysis. With $\alpha = 0.3°$, the experimental limit of the observable radii of the colloids can be roughly estimated to be between 1 and 10 nm at 8050 eV.

3. Data correction procedures and theoretical background

An important point in the data treatment of SAXS measurements in grazing incidence is the correction for absorption and refraction effects. Let I_{incid} be the X-ray intensity arriving at the surface of the sample with $\alpha = 0.3° > \varphi_c$ (see Fig. 4). As α is near to φ_c, refraction of the incident beam at the surface of the sample has to be taken into account. For simplicity, the angle φ', which is additionally necessary to describe the X-ray path in two dimensions, is not shown in Fig. 4. A more detailed drawing of the geometry in two dimensions is given in the *International Tables of X-ray Crystallography* (1989) as well as by Smoluchowski & Turner (1949) and Naudon (1995). For X-rays with $\lambda \simeq 0.1$ nm, the refractive index n is complex and can be written

$$n = 1 - \delta - i\beta \tag{1}$$

with

$$\delta = 2.7019 \times 10^{10} \rho \lambda^2 \sum_i n_i (f_{0,i} + f_i')/\sum_i n_i A_i$$

$$\beta = \lambda/4\pi\rho \sum_i f_i'' n_i = \lambda\mu/4\pi$$

where λ is wavelength (cm), ρ density (g cm^{-3}), $f = f_0 + f' + if''$ atomic scattering factors (Sazaki, 1984) and n_i, Z_i and A_i are atomic concentration, number and mass of species i.

As shown in Fig. 4, the incident primary beam is first partially reflected at the surface of the sample. Within the coating it is then reflected and attenuated by absorption before being scattered under the angle $2\theta'$. The refracted angle α' inside the sample is given by equation (2). The scattered beam is then further absorbed and finally refracted when it leaves the sample. As it enters the detector, by definition under the angle 2θ, the scale of the scattering vector $\mathbf{q} = 4\pi/\lambda \sin\theta$ has to be recalculated after the experiments as the external 2θ scale does not represent the internal angle of diffraction $2\theta'$. The minimal detectable angle of diffraction $2\theta'_{\min}$ of the q scale is then given by $\alpha' + \alpha_c$.

$$\cos(\alpha') = \cos(\alpha)/(1 - \delta)$$

and

$$\cos(2\theta' - \alpha') = \cos(2\theta - \alpha)/(1 - \delta). \tag{2}$$

The correction of the transmitted intensity by absorption has to be done in the two-dimensional representation of the spectra as it leads to a deformation of the detected scattering image, especially for small angles 2θ. The X-ray path L for a photon scattered in a depth z is given by (Smoluchowski & Turner, 1949)

$$L(\alpha', 2\theta', \varphi') = z\{1/\sin(\alpha') + 1/[\sin(2\theta')\sin(\alpha') - \cos(\alpha')\cos(2\theta')\cos(\varphi')]\}. \tag{3}$$

To simplify the two-dimensional absorption correction procedure, the internal angle φ' was replaced by the external angle φ. The effect of this approximation is small and assumes effectively that the cone formed by the scattered beam is only scaled down for transmission correction due to the change from 2θ to $2\theta'$ and not slightly deformed as would be the case if φ' is regarded as a function of $2\theta'$. For a given thickness of the coating t and an X-ray mass absorption coefficient μ (cm^{-1}), the total scattered intensity I_{detec} arriving at the detector of an incident beam I_{incid} with cross-sectional area A is then given by

$$I_{\text{detec}}(\alpha, \alpha', 2\theta, \varphi) = [I_{\text{incid}} A/\sin(\alpha)]\{1 - \exp[\mu t L(\alpha', \theta', \varphi')]\} \times [\mu L(\alpha', \theta', \varphi')]^{-1}. \tag{4}$$

Using equation (4), the intensity I_{incid} has to be recalculated in two dimensions as a function of I_{detec}, 2θ and φ with known parameters α, α', μ and t. The values of μ were calculated from the stoichiometric composition of the coatings and with the help of data from secondary neutral mass spectroscopy (SNMS) measurements. They are known with a relative accuracy of about 10%, which is mainly limited by an increasing loss or burn-out of organic compounds in the coatings with temperature. The thickness of the coatings was determined by ellipsometry (see Table 1) with an accuracy of between 5 and 10%, which is due to diffusion effects at the coating–substrate interface smoothing the originally sharp boundary. A possible deviation of the product μt from its precise value seems to be a crucial point for the trans-

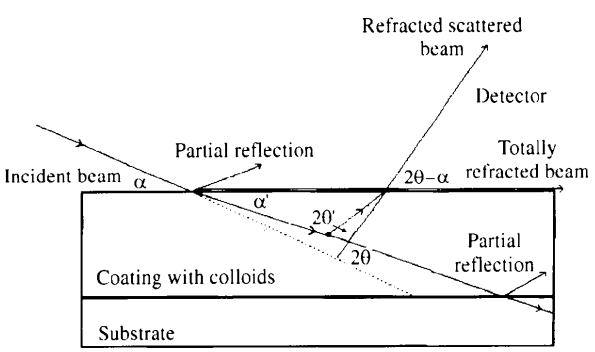

Fig. 4. Schematic one-dimensional representation of the X-ray path in the sample for $\alpha \geqslant \phi_c$ at grazing incidence taking refraction effects into account.

Table 1. *Thickness t (μm) and calculated values of μ (cm^{-1}) for the coatings with and without Au colloids as a function of the densification temperature*

	353 K	423 K	473 K	523 K	573 K
Coating with Au colloids (t, μ)	2.01 42	1.96 48	1.59 57	1.11 68	1.18 76
Coating without colloids (t, μ)	1.97 22	1.93 25	1.55 29	1.06 35	1.21 38

mission correction, but its effect in this case is quite low, as can be seen from the effective X-ray penetration depth in the coatings $I(z_{1/e}) = I(0)/e$. It is calculated by equation (5) (Parrat, 1954; Parrat & Hempstead, 1954) which at $\lambda = 0.154$ nm leads to typical values of $z_{1/e} = 1.0$ to 0.5 μm.

$$z_{1/e} = \lambda/4\pi 2^{1/2}\{[(\alpha^2 - \varphi_c^2)^2 + 4\beta^2]^{1/2} - (\alpha^2 - \varphi_c^2)\}^{-1/2}$$

and

$$1/z_{\text{eff}} = 1/z_{1/e} + 1/z'_{1/e}. \quad (5)$$

A similar formula is valid for the escape depth $z'_{1/e}$ of the diffracted emerging beam. The effective analysis depth z_{eff} is then in all cases half the thickness of the coatings, if not less. Thus, possible errors in μt only have a small influence on the corrections and any intensity contributions from reflections at the interface between coating and substrate will not be detected.

The recorded spectra were finally corrected by equation (6) for detector efficiency with energy and position as well as for incident photon flux and background signal

$$I(\mathbf{q}) \simeq \text{Eff}(E)\text{Eff}(\mathbf{q})[I_{\text{scatt.cor}}(\mathbf{q})/\text{monitoring} - I_{\text{vac}}(\mathbf{q})/\text{monitoring}] \quad (6)$$

where Eff(E) is the variation of the detector efficiency with energy as determined with a foil of an Al_4Ag_{96} alloy, Eff($\mathbf{q}$) the variation of the detector efficiency with position, I_{vac} the background signal of the detector without a sample, $I_{\text{scatt.cor}}$ the intensity after correction for transmission and refraction, and 'monitoring' the incident X-ray intensity as measured simultaneously by a scintillator.

The effective illuminated area for a beam collimated to 0.1 × 1 mm with $\alpha = 0.3°$ is about 19 × 1 mm. Therefore, scattering that occurs under the same angle $2\theta'$ at two different positions perpendicular to the sample surface will not be detected at the same position of the detector. Deviations in 2θ can be approximated by (7) leading to values of $d\theta$ in the range 0.01–0.09°. The detector resolution was about 0.044°.

$$d\theta = h \sin(2\theta - \alpha)/[d \sin(\alpha)]. \quad (7)$$

Test calculations applying standard desmearing procedures (Glatter, 1977, 1980; Paar, 1992) showed that this effect was not easy to resolve. Therefore, this treatment was omitted.

ASAXS experiments are interpreted in this paper in a first approximation by a two-phase model assuming sharp interfaces between matrix and colloids. It can then be written as (Goerigk, Haubold, Klinshirn & Uhrig, 1994)

$$d\sigma/d\Omega(\mathbf{q}, E) = N_{\text{coll}}\Delta\rho^2 V_{\text{coll}}^2 S(\mathbf{q}) \quad \text{and} \quad I(E)^{1/2} \propto \Delta\rho \quad (8)$$

where N_{coll} is the number of colloids within the matrix, $\Delta\rho$ the contrast in electron density, V_{coll} the volume of a single colloid, $S(\mathbf{q})$ the scattering function of a single crystalline particle and $I(E)$ the measured intensity at the energy E.

The contrast $\Delta\rho$ for gold colloids in a matrix with known composition is given by (Simon, Lyon, Buson & Rieutord, 1991)

$$\Delta\rho^2 = |f_{\text{Au colloids}}(E)/V_{\text{Au colloids}} - f_{\text{matrix}}(E)/V_{\text{matrix}}|^2 \quad (9)$$

where

$$f_{\text{Au colloids}}(E) = f_{\text{Au}}(E) \text{ and } f_{\text{matrix}}(E) = \sum_i x_i f_i(E)/\sum_i x_i$$

with i = Si, O, C, N, Cl, H and Au; x_i is the stoichiometric contribution of element i to the matrix composition (in the case of Au only ions/atoms left in the matrix have to be considered); $f_i(E)$ is the atomic scattering factor of the element i at the energy E; $V_{\text{Au colloids}}$ and V_{matrix} are the mean specific volumes of the gold atoms and the matrix atoms, respectively.

The incident X-ray energy was varied to below the L_{III}-absorption edge of Au at 11 919 eV, leading to a strong change in the atomic scattering factor $f'_{\text{Au}}(E)$ of the Au colloids. Below 11 900 eV, the variation of $f'_i(E)$ and $f''_i(E)$ of the other elements as well as that of $f'_{\text{Au}}(E)$ is weak and can be neglected. ASAXS measurements below the absorption edge of Au were performed at 11 637, 11 786, 11 854, 11 887 and 11 903 eV. A typical time taken to obtain one scattering spectrum with a statistical uncertainty of less than 1% was 30 min.

The accuracy of the variation of the contrast $\Delta\rho$ as a function of energy is limited by errors in the stoichiometric composition of the coatings and by gold atoms or complexed gold ions left in the matrix at certain densification temperatures. These do not contribute to the scattering signal but have to be considered in the calculation of $f_{\text{matrix}}(E)$ and $\Delta\rho$. The ratio of gold being transferred into colloids compared with the total amount added to the sol has been evaluated by UV–visible absorbance measurements of the coatings (Fig. 6) which were compared with calculated Mie spectra (Mie, 1908; Fröhlich & Berg, 1982) for a given size and con-

centration of the colloids, bearing in mind that the area of the plasma resonance peak in these spectra is proportional to the volume fraction of gold colloids in the coatings.

4. Description of the samples

For the preparation of the glass-like sol–gel coatings containing gold colloids, 1.0 g of $H(AuCl_4).H_2O$ was dissolved in 15 ml of ethanol. 1.776 ml of [*N*-(2-aminoethyl)-3-aminopropyl]trimethoxysilane (DIAMO) was added to the solution (molar ratio of Au:DIAMO = 1:4). Finally, 18.8 ml of the matrix sol, prepared from 160 ml of 3-glycidoxypropyltriethoxysilane (GPTS) and 40 ml of tetraethylorthosilicate (TEOS), dissolved in 240 ml of ethanol and prehydrolyzed with 28.5 ml of 0.1 *M* HNO_3 was added and stirred for some minutes. A clear and slightly yellow-coloured sol was obtained. Soda-lime glass microscopic slides were then dip-coated with a withdrawal speed of 10 mm s^{-1} and dried at 353 K for 1 h to remove the alcohols from the gel. All coatings showed an intense red colour, which is typical of the absorption of gold colloids. The coatings were finally further densified under ambient air between 423 and 573 K in 50 K steps for 1 h (heating rate 60 K h^{-1}). More detailed information about the preparation of the coatings can be found in the work of Schmitt (1997), Mennig, Becker, Schmitt & Schmidt (1994) and Kutsch, Lyon, Schmitt, Mennig & Schmidt (1997).

For samples densified at 353 K, it was possible to prepare equivalent free-standing films, which were densified only at 353 K. They had a thickness of 0.216 mm and a density of 1.42 g cm^{-3} and were investigated by (A)SAXS using conventional transmission techniques, allowing the comparison of the measured value of μ (37.0 cm^{-1}) directly with the calculated value (38 cm^{-1}). The preparation of similar films with densification temperatures above 423 K was not possible because of growing mechanical stress within the films, leading to their destruction.

The thickness t of the coatings as measured by ellipsometry and the values of μ calculated according to the composition of the coatings [see equation (1)] are summarized in Table 1. The values of δ and β at $E = 8050$ eV, which were used for this calculation, increased with densification temperature from 4.8×10^{-6} to 6.8×10^{-6} and 5.1×10^{-8} to 9.3×10^{-8}, respectively, leading to a critical angle $\varphi_c = (2\delta)^{1/2}$ of about 0.18–0.22° in accordance with the experimental observations. The $f'(E)$ and $f''(E)$ data of the different elements for these calculations were taken from Sazaki (1984).

5. Characterization by UV–visible spectroscopy

The UV–visible absorbance spectra of the coatings (Fig. 5) show in all cases the expected plasma resonance peak of gold colloids. The peak maximum shifts continuously to a slightly higher wavelength with increasing densification temperature, indicating growing nano-scaled particles. The high FWHM (full width at half-maximum) of each peak (generally indicating small colloids) is remarkably larger than expected from theoretical calculations according to Mie theory (Mie, 1908) for sizes between 1 and 10 nm, even if a broad size distribution is assumed. Thus, a precise evaluation of the size of the colloids is not possible from UV–visible spectroscopy. The reason for this unexpected broadening of the peaks is not yet well understood but is strongly dependent on the kind and concentration of the stabilizer used in the sol (Schmitt, 1997) and might be affected by the different dielectric properties of the interface (Hövel, Fritz, Hilger, Kreibig & Vollmer, 1993; Perrson, 1993). In the case of molten glasses containing nano-scaled gold colloids, the agreement between theoretical calculations and measured spectra is in general very good. In fact, the phase boundary between matrix and colloids in the sol–gel coatings is probably not as sharp as assumed in the first approximation applied here. This will be discussed in detail in a future publication and was one motivation for investigating the colloids by SAXS and developing the experimental basis for such experiments in grazing incidence. The volume fraction of gold being reduced by transfer into colloids compared with the total amount of gold added to the sol, assuming a mean size of the colloids of $r = R_g$ and a thickness of the coatings according to Table 1, has been determined by a comparison of calculated Mie spectra with the experimental results. These data, given in Table 2, were used to improve the values of $\Delta\rho$ according to equation (9).

The volume fraction of colloidal gold in the coatings mainly depends on two factors: the densification of the coatings with temperature (increasing mechanic density and growing burn-out of organic components) and the growing amount of colloidal gold in the coatings due to

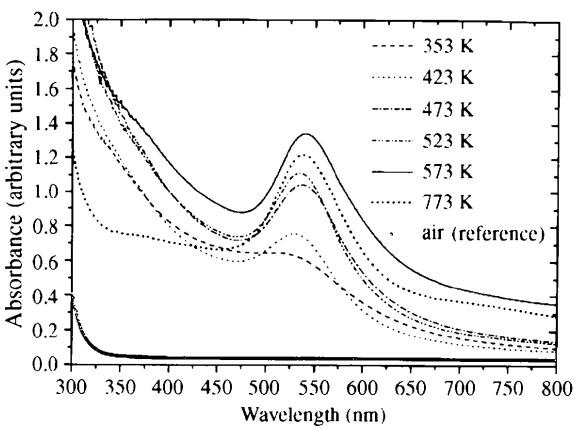

Fig. 5. UV–visible absorbance spectra of coatings densified between 353 and 573 K in air on soda-lime glass substrates (molar ratio Au:DIAMO = 1:4).

Table 2. *Ratio of Au transferred into colloids compared with the total amount of Au added to the sol as determined from UV–visible absorbance spectra as a function of the densification temperature with Au:DIAMO = 1:4 (estimated precision: ± 5%)*

	353 K	423 K	473 K	523 K	573 K	773 K
Ratio (%)	19	18	34	48	63	97

further thermal reduction. The mechanic density of the coatings grows from about 1.3 to 1.5 g cm^{-3} at 853 K (see also results from free-standing films) to about 2.2 g cm^{-3} at 773 K (limit for molten glass). Thus, starting with the known amount of gold ions added to the sol, the volume fraction of colloidal gold in the coatings is calculated to be 0.1–0.2% at 353 K, 0.8–1.2% at 573 K and about 2% at 773 K, taking into account the data given in Table 2. This result shows that the relation $V_{\text{colloids}}/V_{\text{matrix}} \ll 1$ is always fulfilled. Therefore, the mean interparticle distance is much higher than the diameter of the colloids and any interparticle interaction contributions or multiple scattering effects can be neglected in the following interpretation of the SAXS data (Feigin & Svergun, 1987). The SAXS spectra can be treated in a good approximation as the sum of the scattering of isolated individual Au colloids.

6. Characterization by HTEM

In order to confirm the size distribution of the colloids obtained by the SAXS analysis, Figs. 6 and 7 show the results of HTEM experiments on a coating densified at 423 K. The diameters of the colloids in the sample were found to be between 0.5 and 8 nm. Their shapes were generally spherical and they were mostly single crystalline (f.c.c. structure). Most of the particles had a size below $r = 0.5$ nm. Since the low scattering contrast of these particles led to high statistical errors and to the restricted size of the colloids which could be detected by SAXS ($1\text{ nm} < r < 10\text{ nm}$), only colloids with $r > 0.5$ nm were considered in Fig. 7 for the evaluation of the size distribution. In this range it could be fitted roughly by a logarithmic normal distribution. The HTEM results suggest the formation of very small gold nuclei ($r < 0.5$ nm) in a first reduction step and the growth of these particles either by diffusion or coalescence in a second step during densification. Only the latter particles were detected by SAXS.

7. First results of the (A)SAXS experiments

To verify that the observed scattering signals in grazing incidence are only caused by the scattering of gold colloids and are not due to any parasitic diffusion, the X-ray energy below the absorption edge of gold was varied in order to check the linear behaviour predicted by equation (9).

The results of these investigations for five different energies after data corrections are shown in Fig. 8 for coatings densified at 353 and 423 K as well as for a film densified at 353 using the transmission technique. In each case, the expected linear variation could be verified. No significant differences between the coatings and film were observed. The curve in the case of the coating densified at 423 K is slightly displaced because of a growing electronic density of the matrix with densification. Table 3 gives the results of the linear fits indicated in Fig. 8, assuming $[I/I(0)]^{1/2} = \alpha\Delta\rho + \beta$, together with the correlation coefficient R.

Further experiments with nearly equivalent coatings without gold colloids confirmed that the observed scattering signal was due to the gold colloids, as in this case only a very weak scattering signal was detected which was negligible compared with the samples with gold colloids.

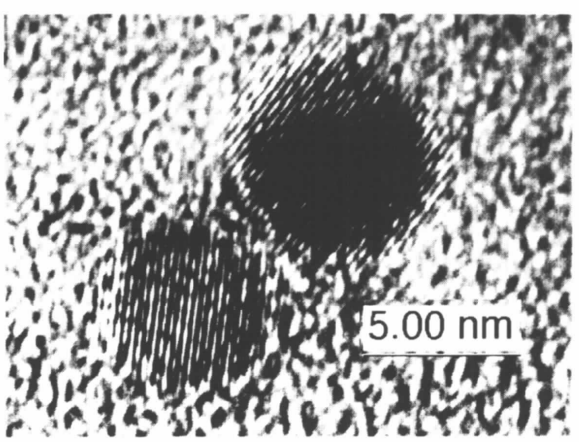

Fig. 6. HTEM picture of single crystalline gold colloids from the coating densified at 423 K (Au:DIAMO = 1:4).

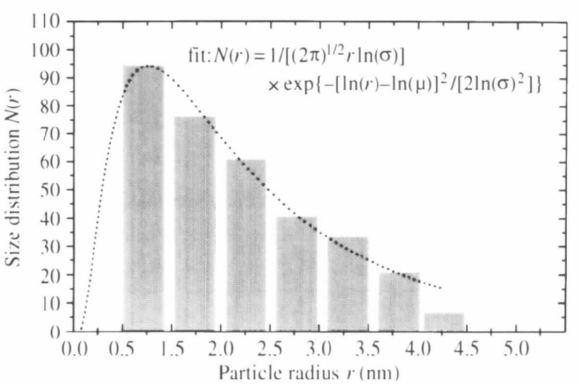

Fig. 7. Size distribution from HTEM (sample: see Fig. 6) for $r > 0.5$ nm and a fit assuming a logarithmic normal distribution. Width of size intervals 0.52 nm, total number of evaluated particles 336, limit of the size evaluation $r > 0.5$ nm.

In order to demonstrate that the correction procedures described in §3 are really necessary to obtain reliable results, Fig. 9 gives the scattering spectra after different steps of correction for a sample densified at 473 K with Au:DIAMO = 1:4 at $E = 8050$ eV in grazing incidence in a $\log(I)$ *versus* q representation. Details of the calculation parameters are given in the plot. The lowest spectrum has only been corrected for detector efficiency and background signal. This was further corrected for transmission and then also for refraction effects. For the purposes of comparison between the fully corrected spectrum and the uncorrected spectrum, the latter has also been scaled-up by its calculated transmission coefficient T. Thus, effects from the transmission correction as a function of q can be directly evaluated. Additionally, Table 4 summarizes the changes in the values of R_g and the Porod exponent m during the different steps.

From Fig. 9 and Table 4, it can be concluded that elaborate correction procedures work reasonably well. They are mandatory especially for the smaller q values in order to obtain reliable results for R_g and for the calculated size distributions. The radii of gyration increased by up to 5% after the corrections. The variation of m, however, seems not to be significant. In particular, the correction for refraction effects leads to an additional cut of the spectra for small q values and to a remarkable change in their shape, which has an important influence on the calculated size distribution of the colloids.

Fig. 10 shows the corrected scattering spectra in the case of coatings densified at 373 to 573 K in grazing incidence at $E = 8050$ eV in a $\log(I)$ *versus* $\log(q)$ representation together with a fit in the clearly visible linear q range in order to evaluate the Porod exponent m given by $I(q) = I(0)q^m$. The radii of gyration R_g were determined from these spectra by linear extrapolation to zero in a $\log(I)$ *versus* q^2 representation. The resulting values of m and R_g, which increased again by several percent after the correction procedures, are summarized in Table 5. The scattering signal from equivalent samples without gold colloids was again very weak. In the case of the film densified at 353 K a value of $R_g = 1.27$ nm and a slope of -3.0 in a well established linear range were additionally evaluated in transmission.

The slopes in the Porod region for high q values as indicated in Fig. 10 (estimated precision ± 0.2) differ significantly from -4, which is to be expected in the case of particles with sharp phase boundaries in a homogeneous matrix. They also indicate clearly a structural change between 353 and 473 K. These results, which will be presented in detail in a further paper along with those for other gold:stabilizer ratios, offer an insight into the electronic structure of the interface between matrix and colloids (Kutsch, Lyon, Schmitt,

Table 3. *Results of the linear fits indicated in Fig. 8 and correlation coefficient R*

	α	β	R
353 K, film in transmission	0.217	0.221	0.979
353 K, coating in grazing incidence	0.227	0.188	0.983
423 K, coating in grazing incidence	0.229	0.197	0.973

Table 4. *Effects of the different correction procedures on the value of the radius of gyration R_g and the Porod exponent m including estimated errors (see Fig. 9)*

	R_g (nm)	m
Without correction for transmission and refraction	4.47 (15)	−4.83 (20)
Including correction for transmission	4.54 (15)	−4.99 (20)
Including correction for transmission and refraction	4.70 (20)	−4.67 (20)

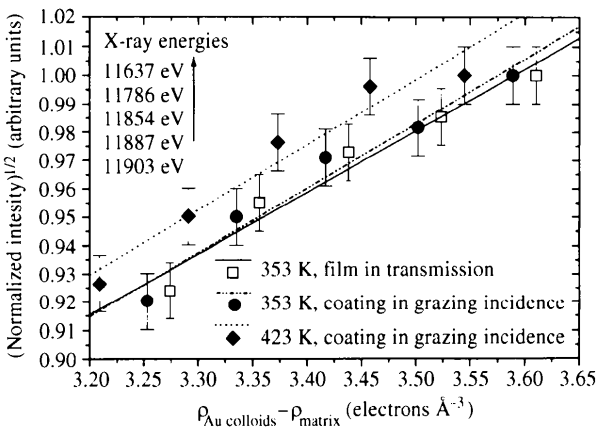

Fig. 8. Variation of the square root of the corrected intensity (normalized at 11 637 eV) as a function of $\Delta\rho$ below the absorption edge of gold for coatings densified at 353 and 423 K (grazing incidence). For comparison, the same variation is also indicated for the film densified at 353 K (transmission) with Au:DIAMO = 1:4.

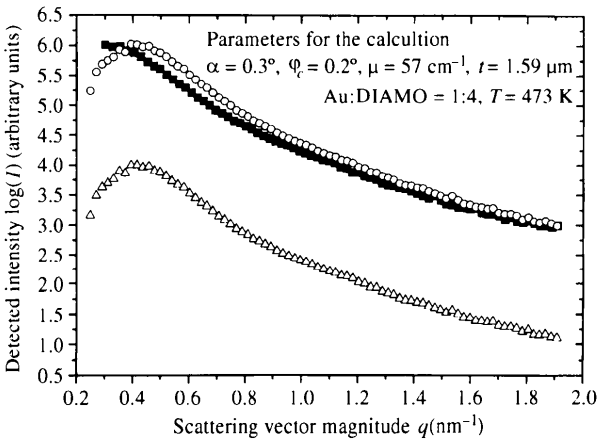

Fig. 9. Variation of scattering spectra during the different correction procecures. △, without correction; ○, only correction for transmission; ■, correction for transmission and refraction.

Mennig & Schmidt, 1997). From Fig. 10, it can be seen that the q range where the linear approximation is valid rises with densification temperature, indicating that the mean size of the gold colloids grows continuously with temperature (*i.e.* by diffusion or coalescence). This growth is also reflected in a continuous transfer of intensity from high to smaller q values. In the case of the sample densified at 353 K, only a part of the scattering of the colloids was detected as the spectra is limited by the angular range covered by the detector. The scattering of very small colloids with radii $r < 1$ nm, which cause a scattering signal at high q values, is not observed in the experiments, leading to errors in the calculated size distribution of the colloids below 1 nm as given in Fig. 11. In this case, the slope of -3.2 in the Porod region also has to be interpreted very carefully, as the linear region is too small to allow its precise determination and as the contribution of the small particles with $r < 1$ nm in the greater q region is not observed. With respect to the size of the colloids ($R_g = 1.38$ nm), it should also be mentioned that the Porod limit was not reached in the q range where the slope was evaluated. The accordance with the data from the free-standing film and with further results published in a second paper (Kutsch, Lyon, Schmitt, Mennig & Schmidt, 1997) we feel is justification for us to present this value in Fig. 10 and Table 5, despite the arguments against its significance.

To calculate the size distribution of the gold colloids within the coatings, the spectra presented in Fig. 10 have been evaluated with commercial software distributed by Paar GmbH (Paar, 1992). This software is based on the work of Glatter (1977, 1980) and Glatter & Hainisch (1984) and uses the indirect transformation method assuming spherical particles, no multiple scattering effects (infinite dilution), random particle distribution, pinhole collimation and monochromatic X-ray radiation;

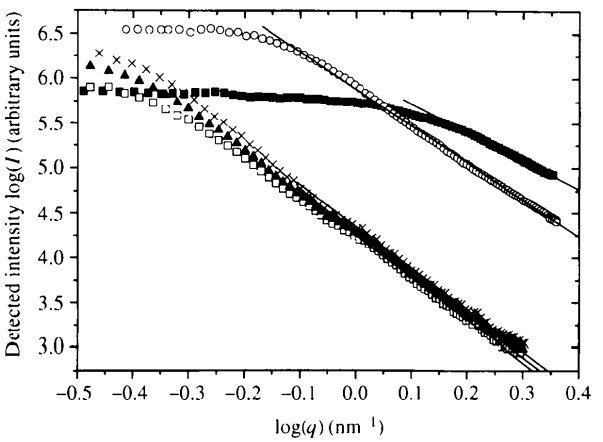

Fig. 10. Determination of the slopes in the linear region of the log(I) *versus* log(q) representation. ■ 353 K, $m = -3.2$ (?); ○ 423 K, $m = -4.1$; □ 473 K, $m = -4.7$; ▲ 523 K, $m = -4.7$; × 573 K, $m = -4.7$. Au:DIAMO = 1:4.

Table 5. *Variation of the radii of gyration R_g (nm) and of the Porod exponent m with densification temperature*

	353 K	423 K	473 K	523 K	573 K
R_g	1.38	3.01	4.70	5.19	5.39
m	−3.2 (?)	−4.1	−4.7	−4.7	−4.7

according to the HTEM investigations and the calculated volume fraction of colloidal gold in the samples (see §5) these criteria are fulfilled in our study. Furthermore, the calculation needs an *a priori* estimation of the limits of the size distribution, which were given here by $r_{min} = 0$, $N(0) = 0$ and $r_{max} > 3R_g$.

The results (Fig. 11) are in good agreement with the evaluated radii of gyration and the size distribution obtained by HTEM as demonstrated in the case of a coating densified at 423 K (Fig. 7). Significant deviations are found for $r < 1$ nm which is below the detectable size range of the SAXS spectra, indicating an inappropriate calculation due to the lack of reliable experimental data. An improvement of the agreement for small colloids can only be achieved by extension of the detected angular range as discussed above. In summary, the rise in the densification temperature clearly leads to a continuous increase in the size of the colloids up to 473 K. Between 473 and 573 K, only small variations in the size of the colloids are observed.

8. Summary

This paper describes an experimental set-up for (A)SAXS experiments in grazing incidence ($\varphi_i = 0.3°$) in order to investigate thin films and coatings which are not accessible by SAXS in a conventional transmission geometry. As an example, sol–gel coatings containing nano-scaled gold colloids have been studied and it was demonstrated that this method can provide useful information about the electronic structure of the colloids

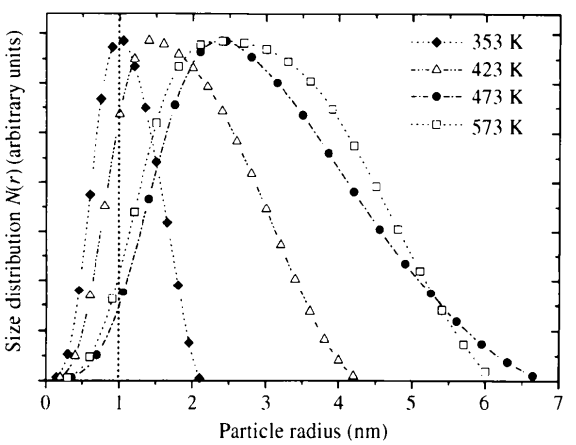

Fig. 11. Normalized size distributions of the colloids for the coatings densified at 353–573 K (Au:DIAMO = 1:4).

and their growth process. In order to correct the spectra obtained by transmission, a new software routine for the data evaluation program at D22 of LURE has been developed. The scattering of the colloids could be clearly identified by ASAXS and it was shown that the size of the colloids can be effectively controlled by the densification temperature and the concentration of the stabilizer. HTEM investigations and UV–visible measurements were in accordance with the SAXS result. In the Porod region of the spectra, slopes were observed which differ significantly from −4. This is thought to be attributable to the interface between matrix and colloids and will be discussed in more detail in a future publication; the gold-to-stabilizer ratios and the influence of other kinds of stabilizers will also be dealt with in a future publication. Further work will concentrate on other noble metal colloids [Cu (Mennig, Schmitt, Kutsch & Schmidt, 1994), Ag, Pd] as well as on higher densification temperatures. Promising results are also expected in the investigation of other sol–gel matrices, such as the $PbO–SiO_2$ system (Schmitt, 1997) which has recently been developed.

This work received financial support from the State of Saarland and the Commission of the European Community under the COMETT program with the participation of EUROMATERIAUX. The authors also thank Dr U. Werner for help with the HTEM investigations.

References

Dubuisson, J. M., Dauvergne, J. M., Depautex, C., Vachette, P. & Williams, C. E. (1986). *Nucl. Instrum. Methods Phys. Res. A*, **246**, 636–640.

Feigin, L. A. & Svergun, D. I. (1987). *Structure Analysis by Small-Angle X-ray Scattering and Neutron Scattering*, ch. 2. New York: Plenum Press.

Fröhlich, M. & Berg, K.-J. (1982). *Phys. Appl.* **9**, 31.

Glatter, O. (1977). *J. Appl. Cryst.* **10**, 415–421.

Glatter, O. (1980). *J. Appl. Cryst.* **13**, 7–11.

Glatter, O. & Hainisch, B. (1984). *J. Appl. Cryst.* **17**, 435–441.

Goerigk, G., Haubold, H.-G., Klinshirn, C. & Uhrig, A. (1994). *J. Appl. Cryst.* **27**, 907–911.

Hövel, H., Fritz, S., Hilger, A., Kreibig, U. & Vollmer, M. (1993). *Phys. Rev. B*, **48**(24), 18178–18188.

International Tables for X-ray Crystallography (1989). Vol. II, edited by T. Hahn, pp. 300–306. Kluwer Academic Publishers.

Kutsch, B., Lyon, O., Schmitt, M., Mennig, M. & Schmidt, H. (1997). *J. Non-Cryst. Solids*. In the press.

Levine, J. R., Cohen, J. B. & Chung, Y. W. (1991). *Surf. Sci.* **248**, 215–224.

Materlik, G., Sparks, C. J. & Fischer, K. (1994). *Resonant Anomalous X-ray Scattering*. Amsterdam: North-Holland.

Mennig, M., Becker, U., Jung, G. & Schmidt, H. (1994). *Sol-Gel Opt. III SPIE*, **2288**, 130–138.

Mennig, M., Becker, U., Schmitt, M. & Schmidt, H. (1994). In *Proceedings of the 8th CIMTEC*, Firenze, Italy, edited by P. Vincenzini. Techna Press.

Mennig, M., Schmitt, M., Kutsch, B. & Schmidt, H. (1994). *Sol-Gel Opt. III SPIE*, **2288**, 120–129.

Mie, G. (1908). *Ann. Phys.* **25**, 377.

Naudon, A. (1995). *Nato ASI Series*, edited by H. Brumberger, Ser. C, vol. 451, pp. 203–220.

Naudon, A., Slimani, T. & Goudeau, P. (1991). *J. Appl. Cryst.* **24**, 501–508.

Paar, A. (1992). Software packages *PDH*92 and *ITP*92. Paar GmbH, 8054 Graz, Austria.

Parrat, L. G. (1954). *Phys. Rev.* **95**(2), 359–369.

Parrat, L. G. & Hempstead, C. F. (1954). *Phys. Rev.* **94**(6), 1593–1600.

Perrson, B. N. J. (1993). *Surf. Sci.* **281**, 153–162.

Sazaki, S. (1984). *Anomalous Scattering Factors*. KEK Report 83-22, Japan.

Schmitt, M. (1997). PhD thesis, Universität des Saarlandes, Germany. In preparation.

Simon, J. P., Lyon, O., Bruson, A. & Rieutord, F. (1991). *J. Appl. Cryst.* **24**, 156–163.

Slimani, T., Goudeau, P., Naudon, A., Farges, G. & Derep, J. L. (1991). *J. Appl. Cryst.* **24**, 638–644.

Smoluchowski, R. & Turner, R. W. (1949). *Rev. Sci. Instrum.* **20**(3), 173–174.

Spanhel, L., Mennig, M. & Schmid, H. (1992). *Bol. Soc. Esp. Ceram.* **VID 31-C**(7), 612–618.